MECHANICS OF COHESIVE-FRICTIONAL MATERIALS
Mech. Cohes.-Frict. Mater. **3**, 343–364 (1998)

On the linearization of the microplane model

Ellen Kuhl and Ekkehard Ramm

Institute of Structural Mechanics, University Stuttgart, Pfaffenwaldring 7, 70550 Stuttgart, Germany

SUMMARY

The paper addresses the microplane model in the context of localization analysis. Capable of reproducing experimental results of concrete specimens, the microplane model includes anisotropic damage in a natural and conceptually simple and explicit way. However, the efficiency of former microplane implementations suffers from the expense of the solution procedure being based on the secant stiffness method. Within this paper, the macroscopic constitutive equation derived by kinematically constraining the microplane strains to the macroscopic strain tensor is consistently linearized resulting in quadratic convergence of the Newton–Raphson iteration for the equilibrium equations. A fully three-dimensional model will be presented and linearized incorporating the two-dimensional case in a natural fashion. Furthermore, the localization criterion is analysed, indicating locally the onset of localization in terms of the acoustic tensor. Several examples demonstrate the features of the microplane model in predicting the material behaviour of concrete in tension and compression as well as in shear. © 1998 John Wiley & Sons, Ltd.

KEY WORDS: concrete modelling; microplane model; anisotropic damage; consistent linearization; localization analysis

1. INTRODUCTION

When subjecting concrete specimens to a load above a certain critical loading situation, microcracks develop in the cement matrix. Number and size of these microcracks grow until the material has reached its load carrying capacity. Strains tend to accumulate locally in small bands giving rise to the formation of macroscopic cracks and stiffness degradation.

This constitutive behaviour of concrete can either be described by softening plasticity (Feenstra[1]), or by the concept of continuum damage mechanics. We will focus on the latter first introduced by Kachanov[2] in 1958 motivated by the idea of a scalar damage variable which can be understood as the ratio of the damaged material area to the initial area. Being composed of a granular material embedded in a cement matrix, concrete has got an extremely heterogeneous microstructure and therefore develops anisotropic damage during loading, which cannot be expressed only by one scalar damage variable. For this reason, concepts of damage formulated in terms of tensors of second, fourth or even eighth order have been introduced as described by Chaboche[3,4] and Lemaitre.[5] Nevertheless, the components of such damage tensors are very difficult to identify.

* Correspondence to: E. Kuhl, Institut für Baustatik, Universität Stuttgart, Pfaffenwaldring 7, D-70550 Stuttgart, Germany.

CCC 1082-5010/98/040343-22$17.50

Received 1 September 1997
Revised 26 January 1998

Bazant and Gambarova[6] have proposed an alternative approach to the tensorial damage formulation, modelling the material behaviour in various different planes through uniaxial stress–strain laws, the so-called microplane model. The concept of considering constitutive laws on special surfaces was originally proposed by Taylor[7] to describe the plastic slip in crystalline materials. Transferred to the method of continuum damage mechanics, the first microplane model was able to cover tension failure. However, the failure modes of cohesive frictional materials cover the wide range from pure mode I failure in tension to mixed mode failure in shear and compression, as already shown by Ros and Eichinger.[8] Therefore, the original microplane model with uniaxial tension laws has been extended by additional uniaxial shear laws on every microplane by Bazant and Prat.[9] No coupling between normal and tangential components has been considered so far, as proposed recently by Iordache and Willam[10] and Weihe *et al.*[11] following the ideas of Otto Mohr. However, a phenomenological dependence of the tangential laws on either the volumetric stress, as proposed by Bazant and Prat,[9] or the volumetric strain, compare Carol *et al.*,[12] has been incorporated. When relating the plane-wise microscopic normal and tangential laws to the macroscale, Carol *et al.*[13] obtain a macroscopic damage formulation in terms of a fourth-order damage tensor, giving physical interpretation to the tensorial components.

The essential drawback of the first implementation of the microplane model was, that the iterative solution procedure of the equilibrium equations was based on the secant stiffness method (Bazant and Ozbolt[14]) such that finding a solution with desired accuracy could take up to a few hundred iteration steps. A later version of the model already included the general expression of the infinitesimal tangent stiffness operator in terms of the values of the three tangent moduli (Carol *et al.*[12]), but the consistent linearization of the overall constitutive relation has been an open problem so far. Therefore, the stress–strain relation will now be linearized resulting in the consistent tangent operator, which guarantees quadratic convergence within a Newton–Raphson solution procedure.

Furthermore, the linearized tangent stiffness operators can be applied to the determination of the acoustic tensor within a localization analysis. When entering the softening regime, materials like concrete exhibit a loss of ellipticity resulting in an ill-posed boundary-value problem with a mesh-dependent solution. The local loss of ellipticity can be analysed through the determinant of the acoustic tensor, as presented in the early work of Hill[15] or more detailed in the context of frictional materials by De Borst.[16]

In section 2, we will explain the ideas of the microplane model, transferring the model to a description in terms of a fourth-order damage tensor. The constitutive relation will be linearized consistently in section 3 leading to an optimal iterative solution procedure of the equilibrium equations in the context of the finite element method. Localization analysis with the help of the acoustic tensor expressed through the consistently linearized tangent moduli is presented in section 4. The numerical examples of a bar in tension and a concrete block of section 5 finally demonstrate the features of the microplane model to capture tension as well as shear failure.

2. THEORY OF THE MICROPLANE MODEL

Anisotropic damage evolution which is characteristic for the material behaviour of concrete can be described by a fourth-order damage formulation. However, it is very difficult to interpret a tensor of fourth order and to identify its components. Within the present section, we will present an alternative interpretation of the damage tensor being composed of scalar-valued damage parameters acting on certain material planes, the so-called microplanes.

Table I. Micro–macro transition

Kinematic constant Voigt	$\longleftarrow \boldsymbol{\varepsilon}$	**Macroscopic scale**	$\boldsymbol{\sigma} \longrightarrow$	Static constraint Reuss
$\varepsilon_{\mathrm{P}}^{I} = \hat{\varepsilon}_{\mathrm{P}}^{I}(\boldsymbol{\varepsilon})$		Localization		$\sigma_{\mathrm{P}}^{I} = \hat{\sigma}_{\mathrm{P}}^{I}(\boldsymbol{\sigma})$
$\downarrow$		**Microscopic scale**		$\downarrow$
$\sigma_{\mathrm{P}}^{I} = \hat{\sigma}_{\mathrm{P}}^{I}(\varepsilon_{\mathrm{P}}^{I})$		Constituive law		$\varepsilon_{\mathrm{P}}^{I} = \hat{\varepsilon}_{\mathrm{P}}^{I}(\sigma_{\mathrm{P}}^{I})$
$\downarrow$		Homogenization		$\downarrow$
$\boldsymbol{\sigma} = \hat{\boldsymbol{\sigma}}(\sigma_{\mathrm{P}}^{I})$	$\longrightarrow \boldsymbol{\sigma}$	**Macroscopic scale**	$\boldsymbol{\varepsilon} \longleftarrow$	$\boldsymbol{\varepsilon} = \hat{\boldsymbol{\varepsilon}}(\varepsilon_{\mathrm{P}}^{I})$

The general idea is to specify the stress–strain relation microscopically on various independent planes in the material, as already introduced by Taylor[7] in 1938. To obtain the material quantities on various planes, a micro–macro transition is necessary. This transition can either be based on a kinematic or on a static constraint. For the case of a kinematic constraint, the strains on each microplane are the resolved components of the macroscopic strain tensor. This approximation which gives an upper bound for the effective moduli has first been established by Voigt in 1989 in the context of homogenization techniques. When a static constraint is applied, however, the stresses on the individual plane are the resolved components of the macroscopic stress tensor. The formulation with a static constraint results in a lower bound for the effective moduli, known as the Reuss bound. Both ways of performing the micro–macro transition are compared in Table I.

The ideas of Taylor were first realized in the slip theory of plasticity based on a static constraint. The dominating failure mechanism described by the slip theory is shear band localization. Bazant and Gambarova[6] have transferred Taylor's idea to the description of tensile fracture of concrete. Their theory which was originally based on the kinematic constraint became well known as the microplane theory. Carol & Prat[17] have applied the static constraint to the microplane model as well, but the decisive disadvantage of the static constraint is its non-uniqueness of active slip systems. In order to avoid this additional difficulty, the microplane approach described in the following is based on a kinematic constraint, see for example the work of Carol *et al.*[12]

2.1. Localization/projection of strains onto the microplane

The following derivation is based on a fully three-dimensional model. However, the reduction to a two-dimensional setting is straightforward. It only influences the tangential components which reduce from a vector format in the three-dimensional model to a scalar if only two dimensions are taken into account.

Restricting the microplane model to small strains, the strain tensor $\boldsymbol{\varepsilon}$ is defined as the symmetric part of the displacement gradient $\nabla\mathbf{u}$:

$$\boldsymbol{\varepsilon} = \nabla^{\mathrm{sym}}\mathbf{u} \tag{1}$$

The normal projection of the macroscopic strain tensor $\boldsymbol{\varepsilon}$ onto each microplane is given by the dyadic product of the normal directions $\mathbf{n}^{\mathrm{I}}$ of the corresponding plane:

$$\varepsilon_{\mathrm{N}}^{I} = \mathbf{n}^{\mathrm{I}} \cdot \boldsymbol{\varepsilon} \cdot \mathbf{n}^{I} = \boldsymbol{\varepsilon} : \mathbf{N}^{I} \quad \text{with } \mathbf{N}^{I} := \mathbf{n}^{I} \otimes \mathbf{n}^{I} \tag{2}$$

In order to differentiate volumetric and deviatoric material behaviour, Bazant and Prat[9] have proposed to split the normal strains ε_N into a normal volumetric part ε_V and a normal deviatoric part ε_D. The volumetric projection, which is the same for each microplane, is given by a third of the trace of the strain tensor $\boldsymbol{\varepsilon}$. The normal deviatoric parts vary from one microplane to the other and can be obtained by substracting the normal volumetric strain ε_V from the total normal projection ε_N^I.

$$\varepsilon_N^I = \varepsilon_V + \varepsilon_D^I \quad \text{with } \varepsilon_V = \boldsymbol{\varepsilon}:\tfrac{1}{3}\mathbf{1} \tag{3}$$

The difference of the strain vector $\boldsymbol{\varepsilon}\cdot\mathbf{n}^I$ and the normal strains ε_N^I multiplied by the corresponding normal direction $\mathbf{n}^I$ defines the R components of the tangential strain vector $\boldsymbol{\varepsilon}_T^{RI}$, see Figure 1. The tangential projection is defined by the third-order tensor $\mathbf{T}^{RI}$ being expressed in terms of the normal $\mathbf{n}$ and the unit tensor of second order 1^{RS}:

$$\varepsilon_T^{RI} = \boldsymbol{\varepsilon}\cdot\mathbf{n}^I - \varepsilon_N^I\mathbf{n}^I = \boldsymbol{\varepsilon}:\mathbf{T}^{RI} \quad \text{with } \mathbf{T}^{RI} = \tfrac{1}{2}(\mathbf{n}^I\mathbf{1}^{JR} + \mathbf{n}^J\mathbf{1}^{IR} - 2\mathbf{n}^I\mathbf{n}^J\mathbf{n}^R) \tag{4}$$

All microscopic components can be obtained by projecting the macroscopic strain tensor with corresponding projection tensors as summarized in the following formulas:

$$\begin{aligned}
\varepsilon_N^I &= \boldsymbol{\varepsilon}:\mathbf{N}^I, & \mathbf{N}^I &:= \mathbf{n}^I \otimes \mathbf{n}^I \\
\varepsilon_V &= \boldsymbol{\varepsilon}:\mathbf{V}, & \mathbf{V} &:= \tfrac{1}{3}\mathbf{1} \\
\varepsilon_D^I &= \boldsymbol{\varepsilon}:\mathbf{D}^I, & \mathbf{D}^I &:= (\mathbf{n}^I \otimes \mathbf{n}^I - \tfrac{1}{3}\mathbf{1}) \\
\varepsilon_T^{RI} &= \boldsymbol{\varepsilon}:\mathbf{T}^{RI}, & \mathbf{T}^{RI} &:= \tfrac{1}{2}(\mathbf{n}^I\mathbf{1}^{JR} + \mathbf{n}^J\mathbf{1}^{IR} - 2\mathbf{n}^I\mathbf{n}^J\mathbf{n}^R)
\end{aligned} \tag{5}$$

Note, that in the two-dimensional case, the tangential strains ε_T^{RI} are scalar valued and can be obtained by omitting the index R. Consequently, the projection tensors $\mathbf{T}^{RI}$ reduce to tensors of second-order $\mathbf{T}^I$, since there is only one tangential direction in a two-dimensional setting.

2.2. *Uniaxial constitutives laws on the microplane*

The volumetric, the deviatoric and the tangential stresses and strains on each microplane are related through the current microscopic constitutive moduli C_V, C_D and C_T. For the model considered here, these moduli are expressed exclusively in terms of the original undamaged moduli C_V^0, C_D^0 and C_T^0 and the individual scalar-valued damage parameters d_V, d_D and d_T, although there are several enhanced models, which also incorporate plastic straining on the

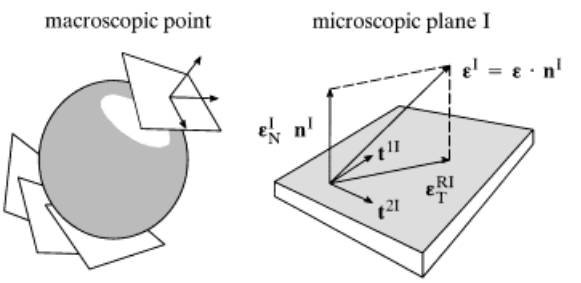

Figure 1. Microplanes in a macroscopic material point

individual microplanes, compare Carol and Bazant,[18] for example. Consequently, the stress components on the microplane I, namely σ_V, σ_D^I and σ_T^{RI}, are given as follows:

$$\begin{aligned} \sigma_V &= C_V \varepsilon_V, & C_V &= (1 - d_V) C_V^0 \\ \sigma_D^I &= C_D^I \varepsilon_D^I, & C_D^I &= (1 - d_D^I) C_D^0 \\ \sigma_T^{RI} &= C_T^I \varepsilon_T^{RI}, & C_T^I &= (1 - d_T^I) C_T^0 \end{aligned} \tag{6}$$

In the following, the so-called 'parallel tangential hypothesis' will be applied according to Bazant and Prat,[9] assuming that the tangential stress vector σ_T^{RI} on each microplane always remains parallel to the corresponding strain vector ε_T^{RI}. With this assumption, the one-dimensional character of the constitutive microplane laws, which is trivially fulfilled for the two-dimensional setting, can be preserved for the three-dimensional case. The tangential damage variable is thus expressed in terms of the norm of the tangential strain vector γ_T^I,

$$d_T^I = \hat{d}_T^I(\gamma_T^I), \qquad \gamma_T^I = \sqrt{\varepsilon_T^{RI} \varepsilon_T^{RI}} \tag{7}$$

compare Carol *et al.*[12] for details. Again, the tangential relation can be simplified to a scalar relation in the two-dimensional case by omitting the direction index R.

The tensorial damage description can now be understood originating from uniaxial stress–strain relations on the microplane. Due to this simplification, the constitutive description of the microplane model gains a physical interpretation and its parameters can be interpreted as damage values in discrete directions.

The scalar-valued damage parameters d_V, d_D and d_T are defined through constitutive laws which differ in compression and tension loading. Damage increases for initial loading whereas it remains constant for unloading and reloading. This corresponds to the well-known concept of macroscopic scalar damage resulting in irreversible stiffness degradation as presented by Lemaitre.[5] In Table II the microplane damage operators for the four different loading cases, tension and the compression as well as loading and un-/reloading are summarized. The case of virgin loading corresponds to the actual value of ε being less than the minimum value reached so

Table II. Microscopic damage operators

	Volumetric part $(1 - d_V)$	Deviatoric part $(1 - d_D^I)$	Tangential part $(1 - d_T^I)$
Tension virgin loading	$\exp\left[-\left[\frac{\varepsilon_V}{a_1}\right]^{p_1}\right]$	$\exp\left[-\left[\frac{\varepsilon_D^I}{a_1}\right]^{p_1}\right]$	$\exp\left[-\left[\frac{\gamma_T^I}{a_3}\right]^{p_3}\right]$
Tension un-/reloading	$\exp\left[-\left[\frac{\varepsilon_V^{\max}}{a_1}\right]^{p_1}\right]$	$\exp\left[-\left[\frac{\varepsilon_D^{I\max}}{a_1}\right]^{p_1}\right]$	$\exp\left[-\left[\frac{\gamma_T^{I\max}}{a_3}\right]^{p_3}\right]$
Compression virgin loading	$\left[\left(1-\frac{\varepsilon_V}{a}\right)^{-p}+\left(-\frac{\varepsilon_V}{b}\right)^{q}\right]$	$\exp\left[-\left[\frac{\varepsilon_D^I}{a_2}\right]^{p_1}\right]$	$\exp\left[-\left[\frac{\gamma_T^I}{a_3}\right]^{p_3}\right]$
Compression un-/reloading	$\left[\left(1-\frac{\varepsilon_V^{\min}}{a}\right)^{-p}+\left(-\frac{\varepsilon_V^{\min}}{b}\right)^{q}\right]$	$\exp\left[-\left[\frac{-\varepsilon_D^{I\min}}{a_2}\right]^{p_2}\right]$	$\exp\left[-\left[\frac{\gamma_T^{I\max}}{a_3}\right]^{p_3}\right]$

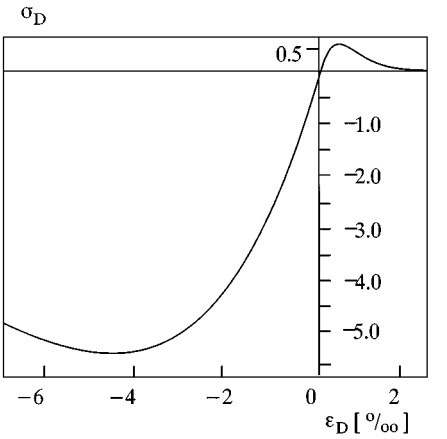

Figure 2. Microscopic normal deviatoric stress–strain law

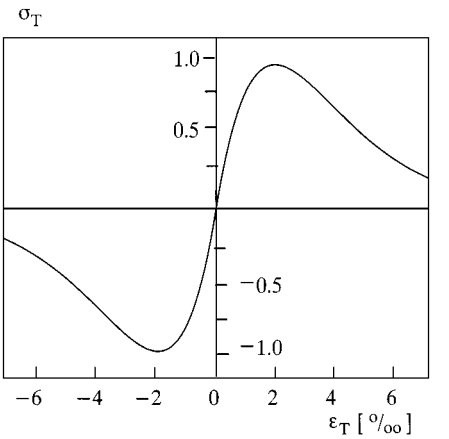

Figure 3. Microscopic tangential stress–strain law

far $\varepsilon^{\min}$ in compression or to ε being larger than the maximum value $\varepsilon^{\max}$ obtained so far in tension, respectively. Consequently, only virgin loading results in damage growth. History dependence is thus reflected through the current minimum and maximum values, which have to be stored as internal variables during the computation.

The damage variables depend on 10 microscopic parameters, namely a, b, p, q, a_1, a_2, a_3, p_1, p_2 and p_3. The resulting microscopic stress–strain laws are presented in Figures 2 and 3. The curves for the example are based on a parameter set found by Bazant and Ozbolt[14] which is given in Section 5. Since the normal volumetric and the normal deviatoric law are identical in tension and differ only slightly in compression, only the deviatoric law is presented in Figure 2.

In contrast to the normal laws, the tangential law is antisymmetric as can be seen in Figure 3. Loading in either direction, negative or positive, causes the same amount of tangential damage on the microplane and results in the same microscopic stiffness degradation. Obviously, for the

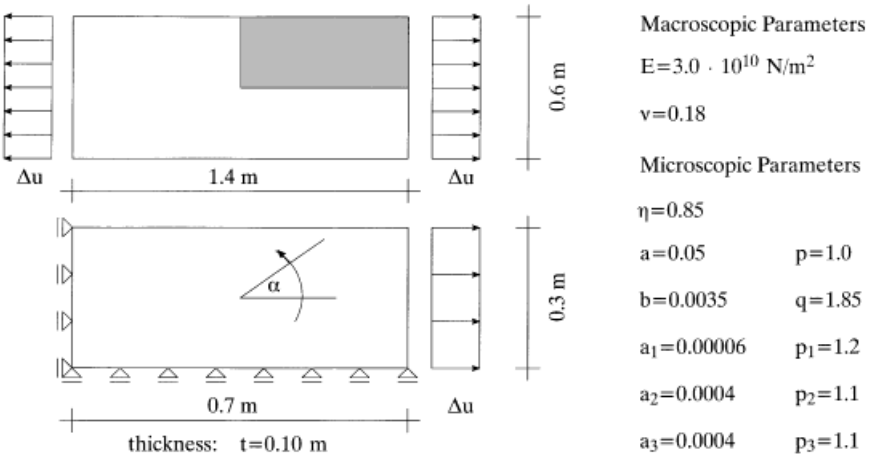

Figure 4. Geometry and parameters of Example 1

chosen set of parameters, the tangential strain belonging to the maximum stress state is about 5 times higher than the critical volumetric and deviatoric strain in tension. It is, however, smaller than the critical volumetric and deviatoric strain in compression which indicates, that in tension failure will occur mainly due to mode I whereas in compression, the structure will rather fail in a mixed mode.

An analysis of global cyclic loading is not considered within this context. A more detailed description on the behaviour of concrete under cyclic loading conditions is given by Ozbolt.[19] However, local unloading of certain integration points will arise, although the load on the global structure increases.

2.3. *Homogenization/determination of macroscopic stresses*

The macroscopic stress tensor can be identified in terms of the microscopic stress components by applying the principle of virtual work. The macroscopic internal virtual work can be expressed as the scalar product of the macroscopic stresses $\boldsymbol{\sigma}$ and a the virtual macroscopic strains $\delta\boldsymbol{\varepsilon}$ multiplied by the surface of the unitsphere:

$$W^{\text{macro}} = \frac{4\Pi}{3}\boldsymbol{\sigma}:\delta\boldsymbol{\varepsilon} \tag{8}$$

Analogously, the microscopic virtual work can be obtained by the sum of all microscopic stress components σ_{N} and σ_{T} multiplied with the corresponding virtual microscopic strain components $\delta\varepsilon_{\text{N}}$ and $\delta\varepsilon_{\text{T}}$ integrated over the unitsphere, denoted by Ω:

$$W^{\text{micro}} = \int_{\Omega} [\sigma_{\text{N}}\delta\varepsilon_{\text{N}} + \sigma_{\text{T}}\delta\varepsilon_{\text{T}}]\,\mathrm{d}\Omega \tag{9}$$

Equivalence of macroscopic and microscopic virtual work yields the macroscopic stress tensor as an integral of the projections of the microplane stress components:

$$\boldsymbol{\sigma}:\delta\boldsymbol{\varepsilon} = \frac{3}{4\Pi}\int_{\Omega} [\sigma_{\text{N}}\delta\varepsilon_{\text{N}} + \sigma_{\text{T}}\delta\varepsilon_{\text{T}}]\,\mathrm{d}\Omega \tag{10}$$

The variations of the microscopic strains can again be expressed in terms of the macroscopic strains with the help of equation (5), based on the idea of the kinematic constraint:

$$\boldsymbol{\sigma}:\delta\boldsymbol{\varepsilon} = \frac{3}{4\Pi}\int_{\Omega}[(\sigma_{\mathrm{V}} + \sigma_{\mathrm{D}})\mathbf{N} + \sigma_{\mathrm{T}}\mathbf{T}]:\delta\boldsymbol{\varepsilon}\,\mathrm{d}\Omega \quad \forall\delta\boldsymbol{\varepsilon} \tag{11}$$

Since the $\delta\boldsymbol{\varepsilon}$ are arbitrary variations of the strains, they can now be eliminated. The integral over the unitsphere can be approximated numerically by the sum of the functions at discrete integration points on the surface of the unitsphere weighted by the coefficients w^I. Theoretically, an infinite number of integration points needs to be considered in each individual material point. In numerical calculations, however, only a discrete number of integration points, denoted by nmp, are examined. In the context of the microplane model, each of the nmp integration points corresponds to one microplane.

$$\boldsymbol{\sigma} = \sigma_{\mathrm{V}}\mathbf{1} + \sum_{I=1}^{\mathrm{nmp}}\sigma_{\mathrm{D}}^{I}\mathbf{N}^{I}w^{I} + \sum_{I=1}^{\mathrm{nmp}}\sigma_{\mathrm{T}}^{RI}\mathbf{T}^{RI}w^{I} \tag{12}$$

For a numerical integration in a two-dimensional simulation, these integration points given through the vectors $\mathbf{n}^I$ describe the surface of a unit circle and are of equal weight:

$$\mathbf{n}^I = [\cos\alpha^I, \sin\alpha^I]^{\mathrm{T}}, \quad \forall I = 1,\ldots,\mathrm{nmp},\ \alpha^{\mathrm{I}} = I\frac{360^\circ}{\mathrm{nmp}} \tag{13}$$

$$w^I = \frac{1}{\mathrm{nmp}}, \quad \forall I = 1,\ldots,\mathrm{nmp}$$

The numerical integration for the three-dimensional case has to be performed over the unitsphere, which is described in detail by Bazant and Oh.[20] For acceptable results at least 42 integration points over the sphere are needed. Their optimal positions and weight coefficients have been examined by Stroud.[21]

The microplane model derived above can easily be transferred into a fourth-order damage model as first proposed by Carol *et al.*[13] Within this contribution, the transformation will be based on the concept of strain equivalence. Other versions like the concept of energy equivalence are described by Carol and Bazant.[18] Replacing the microscopic stresses in formula (12) with the help of help of equations (5) and (6) yields the direct relation between the macroscopic stresses and the macroscopic strains:

$$\boldsymbol{\sigma} = \tilde{\mathbf{E}}:\boldsymbol{\varepsilon} \tag{14}$$

Herein, $\tilde{\mathbf{E}}$ denotes the non-symmetric elasticity tensor modified due to damage. It is given as a sum of the projections of the microscopic constitutive relations in the following form:

$$\tilde{\mathbf{E}} := (1 - d_{\mathrm{V}})C_{\mathrm{V}}^{0}\mathbf{1}\otimes\mathbf{V} + \sum_{I=1}^{\mathrm{nmp}}(1 - d_{\mathrm{D}}^{I})C_{\mathrm{D}}^{0}\mathbf{N}^{I}\otimes\mathbf{D}^{I}w_{I} + \sum_{I=1}^{\mathrm{nmp}}(1 - d_{\mathrm{T}}^{I})C_{\mathrm{T}}^{0}\mathbf{T}^{RI}\otimes\mathbf{T}^{RI}w_{I} \tag{15}$$

The values of the microscopic constitutive parameters C_{V}^{0}, C_{D}^{0} and C_{T}^{0} introduced in equation (6) can now be expressed through the macroscopic values of Young's modulus E and Poisson's ratio

Table III. Microplane damage—constitutive equations

Kinematics	$\boldsymbol{\varepsilon} = \nabla^{\mathrm{sym}}\mathbf{u}$
Microplane Kinematics	$\varepsilon_{\mathrm{V}} = \boldsymbol{\varepsilon}:\mathbf{V}$ $\quad \varepsilon_{\mathrm{D}}^{I} = \boldsymbol{\varepsilon}:\mathbf{D}^{I}$ $\quad \varepsilon_{\mathrm{T}}^{RI} = \boldsymbol{\varepsilon}:\mathbf{T}^{RI}$
Stress	$\boldsymbol{\sigma} = \sigma_{\mathrm{V}}\mathbf{1} + \sum_{I=1}^{\mathrm{nmp}} \sigma_{\mathrm{D}}^{I}\mathbf{N}^{I}w^{I} + \sum_{I=1}^{\mathrm{nmp}} \sigma_{\mathrm{T}}^{RI}\mathbf{T}^{RI}w^{I}$
Microplane stresses	$\sigma_{\mathrm{V}} = (1-d_{\mathrm{V}})C_{\mathrm{V}}^{0}\varepsilon_{\mathrm{V}}$
	$\sigma_{\mathrm{D}}^{I} = (1-d_{\mathrm{D}}^{I})C_{\mathrm{D}}^{0}\varepsilon_{\mathrm{D}}^{I}$
	$\sigma_{\mathrm{T}}^{RI} = (1-d_{\mathrm{T}}^{I})C_{\mathrm{T}}^{0}\varepsilon_{\mathrm{T}}^{RI}$
Damage	$\mathbf{D} = \mathbf{I}^{(4)} - \tilde{\mathbf{E}}:\mathbf{E}^{\mathrm{el}-1}$ $\quad \boldsymbol{\sigma} = \tilde{\mathbf{E}}:\boldsymbol{\varepsilon}$
	$\tilde{\mathbf{E}} = (1-d_{\mathrm{V}})C_{\mathrm{V}}^{0}\mathbf{1}\otimes\mathbf{V} + \sum_{I=1}^{\mathrm{nmp}}(1-d_{\mathrm{D}}^{I})C_{\mathrm{D}}^{0}\mathbf{N}^{I}\otimes\mathbf{D}^{I}w^{I} + \sum_{I=1}^{\mathrm{nmp}}(1-d_{\mathrm{T}}^{I})C_{\mathrm{T}}^{0}\mathbf{T}^{RI}\otimes\mathbf{T}^{RI}w^{I}$
Microplane damage	$d_{\mathrm{V}} = \hat{d}_{\mathrm{V}}(\varepsilon_{\mathrm{V}}),\quad d_{\mathrm{D}}^{I} = \hat{d}_{\mathrm{D}}^{I}(\varepsilon_{\mathrm{D}}),\quad d_{\mathrm{T}}^{I} = \hat{d}_{\mathrm{T}}^{I}(\varepsilon_{\mathrm{T}})$

ν, such that the microplane material operator for undamaged material presented in (15) is identical to the elastic material operator $\mathbf{E}^{\mathrm{el}}$ expressed in terms of E and ν:

$$\begin{aligned}\mathbf{E}^{\mathrm{el}} &= C_{\mathrm{V}}^{0}\mathbf{1}\otimes\mathbf{V} + C_{\mathrm{D}}^{0}\sum_{I=1}^{\mathrm{nmp}}\mathbf{N}^{I}\otimes\mathbf{D}^{I}w^{I} + C_{\mathrm{T}}^{0}\sum_{I=1}^{\mathrm{nmp}}\mathbf{T}^{RI}\otimes\mathbf{T}^{RI}w^{I}\\ &= \frac{E}{1+\nu}\mathbf{I}^{(4)} + \frac{E\nu}{(1+\nu)(1-2\nu)}\mathbf{1}\otimes\mathbf{1}\end{aligned} \tag{16}$$

Consequently, the values of the microscopic constitutive parameters C_{V}^{0}, C_{D}^{0} and C_{T}^{0} are given as follows, with η being a weight coefficient which can be chosen between $0 \leqslant \eta \leqslant 1$:

$$\begin{aligned}C_{\mathrm{V}}^{0} &= \frac{E}{1-2\nu}\\ C_{\mathrm{D}}^{0} &= \frac{\eta E}{1-2\nu}\\ C_{\mathrm{T}}^{0} &= \frac{1}{3}\left[\frac{5-(1-2\nu)}{1+\nu} - 2\eta\right]\frac{E}{1-2\nu}\end{aligned} \tag{17}$$

With the help of equation (15), a fourth-order damage tensor can easily be determined in terms of the scalar-valued damage variables in the well-known format given for example by Lemaitre.[5]

$$\mathbf{D} = \hat{\mathbf{D}}(d_{\mathrm{V}}, d_{\mathrm{D}}^{I}, d_{\mathrm{T}}^{I}) = \mathbf{I}^{(4)} - \tilde{\mathbf{E}}\mathbf{E}^{\mathrm{el}-1}. \tag{18}$$

For the initially undamaged material, the microscopic damage variables are equal to zero and $\tilde{\mathbf{E}}$ is equal to the elasticity tensor $\mathbf{E}^{\mathrm{el}}$. The corresponding fourth-order damage tensor $\mathbf{D}$ is equal to $\mathbf{0}$. For a fully damaged material with the microscopic damage variables all being equal to 1, $\tilde{\mathbf{E}}$ is equal to $\mathbf{0}$ and $\mathbf{D}$ is equal to the fourth-order identity tensor. However, there is no need to determine this damage tensor explicitly within the calculation since the modified elasticity tensor $\tilde{\mathbf{E}}$ can be calculated directly from the microscopic damage variables. The constitutive relations defining the microplane model with kinematic constraint are summarized in Table III.

3. LINEARIZATION OF THE CONSTITUTIVE RELATION

The non-linear system of equations is solved by a Newton–Raphson iteration scheme. In order to guarantee quadratic convergence within the iteration, the constitutive relation has to be linearized consistently. Former implementations of the microplane model are based on the initial stiffness method (Bazant and Ozbolt[14]). Often more than a hundred iteration steps are necessary, to satisfy the equilibrium equations with a desired accuracy. When a Newton–Raphson method is applied, however, only four or five iteration steps are needed. Furthermore, the determination of the tangential stiffness matrix is essential to calculate the acoustic tensor in the localization analysis as described in section 4.

The macroscopic stresses and strains are related by the current constitutive tensor $\tilde{\mathbf{E}}$, which can be interpreted as the initial elastic tensor modified due to damage as defined in equation (14):

$$\boldsymbol{\sigma} = \tilde{\mathbf{E}} : \boldsymbol{\varepsilon}$$

The modified elasticity tensor $\tilde{\mathbf{E}}$ given in equation (15) is obtained by the summation of the actual constitutive moduli multiplied by the dyadic product of the corresponding projections tensors $\mathbf{1}$, $\mathbf{V}$, $\mathbf{N}^I$, $\mathbf{D}^I$ and $\mathbf{T}^{RI}$, respectively,

$$\tilde{\mathbf{E}} = C_{\mathrm{V}} \mathbf{1} \otimes \mathbf{V} + \sum_{I=1}^{\mathrm{nmp}} C_{\mathrm{D}}^I \mathbf{N}^I \otimes \mathbf{D}^I w^I + \sum_{I=1}^{\mathrm{nmp}} C_{\mathrm{T}}^I \mathbf{T}^{RI} \otimes \mathbf{T}^{RI} w^I$$

The linearization of the tensor $\tilde{\mathbf{E}}$, yields the tensor of the tangent moduli $\tilde{\mathbf{E}}^{\mathrm{lin}}$, relating the incremental macroscopic stresses $\Delta\boldsymbol{\sigma}$ to the incremental macroscopic strains $\Delta\boldsymbol{\varepsilon}$.

$$\Delta\boldsymbol{\sigma} = \tilde{\mathbf{E}}^{\mathrm{lin}} : \Delta\boldsymbol{\varepsilon} \quad \text{with } \tilde{\mathbf{E}}^{\mathrm{lin}} := \frac{\partial \boldsymbol{\sigma}}{\partial \boldsymbol{\varepsilon}} \tag{19}$$

It can be obtained by calculating the corresponding Gâteaux derivative given in the following form:

$$\tilde{\mathbf{E}}^{\mathrm{lin}} : \Delta\boldsymbol{\varepsilon} = \frac{\mathrm{d}}{\mathrm{d}\eta} [\hat{\boldsymbol{\sigma}}(\boldsymbol{\varepsilon} + \eta\Delta\boldsymbol{\varepsilon})]_{\eta=0} \tag{20}$$

Applying the definition of the macroscopic stresses (12), the following relation can be obtained:

$$\begin{aligned} \tilde{\mathbf{E}}^{\mathrm{lin}} : \Delta\boldsymbol{\varepsilon} = {} & \frac{\mathrm{d}}{\mathrm{d}\eta} [\hat{\sigma}_{\mathrm{V}}(\boldsymbol{\varepsilon} + \eta\Delta\boldsymbol{\varepsilon})\mathbf{1}]_{\eta=0} + \frac{\mathrm{d}}{\mathrm{d}\eta} \left[\sum_{I=1}^{\mathrm{nmp}} \hat{\sigma}_{\mathrm{D}}^I (\boldsymbol{\varepsilon} + \eta\Delta\boldsymbol{\varepsilon}) \mathbf{N}^I w^I \right]_{\eta=0} \\ & + \frac{\mathrm{d}}{\mathrm{d}\eta} \left[\sum_{I=1}^{\mathrm{nmp}} \hat{\sigma}_{\mathrm{T}}^{RI} (\boldsymbol{\varepsilon} + \eta\Delta\boldsymbol{\varepsilon}) \mathbf{T}^{RI} w^I \right]_{\eta=0} \end{aligned} \tag{21}$$

It is obvious, that the linearization formula consists of three terms, the volumetric, the deviatoric and the tangential part:

$$\tilde{\mathbf{E}}^{\mathrm{lin}} : \Delta\boldsymbol{\varepsilon} = \tilde{\mathbf{E}}_{\mathrm{V}}^{\mathrm{lin}} : \Delta\boldsymbol{\varepsilon} + \tilde{\mathbf{E}}_{\mathrm{D}}^{\mathrm{lin}} : \Delta\boldsymbol{\varepsilon} + \tilde{\mathbf{E}}_{\mathrm{T}}^{\mathrm{lin}} : \Delta\boldsymbol{\varepsilon} \tag{22}$$

In the following, we will describe the linearization procedure of the first term, which is the volumetric part of the linearized modified elasticity tensor $\tilde{\mathbf{E}}_{\mathrm{V}}^{\mathrm{lin}}$. The linearizations of the other

terms can be performed analogously. With the definition of the microscopic stresses (6) the first term of equation (22) can be expressed as

$$\tilde{\mathbf{E}}_{\mathrm{V}}^{\mathrm{lin}}:\Delta\boldsymbol{\varepsilon} = \frac{\mathrm{d}}{\mathrm{d}\eta}[(1-\hat{d}_{\mathrm{V}}(\boldsymbol{\varepsilon}+\eta\Delta\boldsymbol{\varepsilon}))C_{\mathrm{V}}^{0}\hat{\varepsilon}_{\mathrm{V}}(\boldsymbol{\varepsilon}+\eta\Delta\boldsymbol{\varepsilon})\mathbf{1}]_{\eta=0} \tag{23}$$

The volumetric strain ε_{V} is given through equation (5) in the following form:

$$\varepsilon_{\mathrm{V}} = \hat{\varepsilon}_{\mathrm{V}}(\boldsymbol{\varepsilon}+\eta\Delta\boldsymbol{\varepsilon}) = (\boldsymbol{\varepsilon}+\eta\Delta\boldsymbol{\varepsilon}):\mathbf{V} \tag{24}$$

Assuming the case of virgin tension loading, the volumetric damage operator $(1-d_{\mathrm{V}})$ can be replaced by its definition given in Table II:

$$1-d_{\mathrm{V}} = 1-\hat{d}_{\mathrm{V}}(\boldsymbol{\varepsilon}+\eta\Delta\boldsymbol{\varepsilon}) = \exp\left[-\left[\frac{(\boldsymbol{\varepsilon}+\eta\Delta\boldsymbol{\varepsilon}):\mathbf{V}}{a_1}\right]^{p_1}\right], \quad d_{\mathrm{V}}>0,\ \Delta\varepsilon_{\mathrm{V}}>0 \tag{25}$$

Consequently, with the help of (24) and (25), equation (23) can be written as follows:

$$\tilde{\mathbf{E}}_{\mathrm{V}}^{\mathrm{lin}}:\Delta\boldsymbol{\varepsilon} = \frac{\mathrm{d}}{\mathrm{d}\eta}\left[\exp\left[-\left[\frac{(\boldsymbol{\varepsilon}+\eta\Delta\boldsymbol{\varepsilon}):\mathbf{V}}{a_1}\right]^{p_1}\right]\cdot(\boldsymbol{\varepsilon}+\eta\Delta\boldsymbol{\varepsilon})\right]_{\eta=0} C_{\mathrm{V}}^{0}\mathbf{1}\otimes\mathbf{V} \tag{26}$$

Applying the product formula, one obtains the following compact form for the linearized volumetric modulus in the case of virgin tension loading:

$$\tilde{\mathbf{E}}_{\mathrm{V}}^{\mathrm{lin}}:\Delta\boldsymbol{\varepsilon} = \left[\exp\left[-\left[\frac{\varepsilon_{\mathrm{V}}}{a_1}\right]^{p_1}\right]\left[1-\left[\frac{\varepsilon_{\mathrm{V}}}{a_1}\right]^{p_1}p_1\right]C_{\mathrm{V}}^{0}\mathbf{1}\otimes\mathbf{V}\right]:\Delta\boldsymbol{\varepsilon} \tag{27}$$

The linearization procedure can be understood as a linearization of the damage operator $(1-d_{\mathrm{V}})$ such that

$$\tilde{\mathbf{E}}_{\mathrm{V}}^{\mathrm{lin}} = (1-d_{\mathrm{V}})^{\mathrm{lin}}C_{\mathrm{V}}^{0}\mathbf{1}\otimes\mathbf{V} \tag{28}$$

with the linearized damage operator given in the following form:

$$(1-d_{\mathrm{V}})^{\mathrm{lin}} = \exp\left[-\left[\frac{\varepsilon_{\mathrm{V}}}{a_1}\right]^{p_1}\right]\left[1-\left[\frac{\varepsilon_{\mathrm{V}}}{a_1}\right]^{p_1}p_1\right] \tag{29}$$

The linearizations of the other damage operators can be performed the same way. Their results are summarized in Table IV. The structure of the linearized moduli is thus similar to the continuous moduli presented in equation (15). Obviously, the tangent moduli $\tilde{\mathbf{E}}^{\mathrm{lin}}$ are obtained from the continuous moduli $\tilde{\mathbf{E}}$ by replacing the damage operators $(1-d_{\mathrm{V}})$, $(1-d_{\mathrm{D}}^{I})$ and $(1-d_{\mathrm{T}}^{I})$ by their linearized counterparts:

$$\begin{aligned}\tilde{\mathbf{E}}^{\mathrm{lin}} := {} & (1-d_{\mathrm{V}})^{\mathrm{lin}}C_{\mathrm{V}}^{0}\mathbf{1}\otimes\mathbf{V} + \sum_{I=1}^{\mathrm{nmp}}(1-d_{\mathrm{D}}^{I})^{\mathrm{lin}}C_{\mathrm{D}}^{0}\mathbf{N}^{I}\otimes\mathbf{D}^{I}w_{I} \\ & + \sum_{I=1}^{\mathrm{nmp}}(1-d_{\mathrm{T}}^{I})^{\mathrm{lin}\,RS}C_{\mathrm{D}}^{0}\mathbf{T}^{RI}\otimes\mathbf{T}^{SI}w_{I}\end{aligned} \tag{30}$$

Note, that the for general three-dimensional case, the linearized damage operator of the tangential direction becomes a second-order tensor indicated by the indices R and S, which can again be omitted for the two-dimensional case.

Table IV. Linearized microscopic damage operators

	Volumetric part $(1-d_{\mathrm{V}})^{\mathrm{lin}}$	Deviatoric part $(1-d_{\mathrm{D}}^{I})^{\mathrm{lin}}$	Tangential part $(1-d_{\mathrm{T}}^{I})^{\mathrm{lin}\,RS}$
Tension virgin loading	$\exp\left[-\left[\frac{\varepsilon_{\mathrm{V}}}{a_1}\right]^{p_1}\right]$	$\exp\left[-\left[\frac{\varepsilon_{\mathrm{D}}^{I}}{a_1}\right]^{p_1}\right]$	$\exp\left[-\left[\frac{\gamma_{\mathrm{T}}^{I}}{a_3}\right]^{p_3}\right]$
	$\left[1-\left[\frac{\varepsilon_{\mathrm{V}}}{a_1}\right]^{p_1}p_1\right]$	$\left[1-\left[\frac{\varepsilon_{\mathrm{D}}^{I}}{a_1}\right]^{p_1}p_1\right]$	$\left[1^{RS}-\left[\frac{\gamma_{\mathrm{T}}^{I}}{a_3}\right]^{p_3}p_3\frac{\varepsilon_{\mathrm{T}}^{RI}\varepsilon_{\mathrm{T}}^{SI}}{(\gamma_{\mathrm{T}}^{I})^2}\right]$
Tension un-/reloading	$\exp\left[-\left[\frac{\varepsilon_{\mathrm{V}}^{\max}}{a_1}\right]^{p_1}\right]$	$\exp\left[-\left[\frac{\varepsilon_{\mathrm{D}}^{I\max}}{a_1}\right]^{p_1}\right]$	$\exp\left[-\left[\frac{\gamma_{\mathrm{T}}^{I\max}}{a_3}\right]^{p_3}\frac{\varepsilon_{\mathrm{T}}^{RI}\varepsilon_{\mathrm{T}}^{SI}}{(\gamma_{\mathrm{T}}^{I})^2}\right]$
Compression virgin loading	$\left(1-\frac{\varepsilon_{\mathrm{V}}}{a}\right)^{-p}\left[1+p\left[\frac{\varepsilon_{\mathrm{V}}}{a}-1\right]\right]$	$\exp\left[-\left[\frac{\varepsilon_{\mathrm{D}}^{I}}{a_2}\right]^{p_1}\right]$	$\exp\left[-\left[\frac{\gamma_{\mathrm{T}}^{I}}{a_3}\right]^{p_3}\right]$
	$+\left[-\frac{\varepsilon_{\mathrm{V}}}{b}\right]^{q}[1+q]$	$\left[1-\left[\frac{\varepsilon_{\mathrm{D}}^{I}}{a_2}\right]^{p_2}p_2\right]$	$\left[1^{RS}-\left[\frac{\gamma_{\mathrm{T}}^{I}}{a_3}\right]^{p_3}p_3\frac{\varepsilon_{\mathrm{T}}^{RI}\varepsilon_{\mathrm{T}}^{SI}}{(\gamma_{\mathrm{T}}^{I})^2}\right]$
Compression un-/reloading	$\left[\left(1-\frac{\varepsilon_{\mathrm{V}}^{\min}}{a}\right)^{-p}+\left(-\frac{\varepsilon_{\mathrm{V}}^{\min}}{b}\right)^{q}\right]$	$\exp\left[-\left[\frac{-\varepsilon_{\mathrm{D}}^{I\min}}{a_2}\right]^{p_2}\right]$	$\exp\left[-\left[\frac{\gamma_{\mathrm{T}}^{I\max}}{a_3}\right]^{p_3}\frac{\varepsilon_{\mathrm{T}}^{RI}\varepsilon_{\mathrm{T}}^{SI}}{(\gamma_{\mathrm{T}}^{I})^2}\right]$

For sake of computational convenience, Carol *et al.*[12] have suggested to symmetrize the constitutive relation, which would result in the following form for the symmetrized tangent operator $(\tilde{\mathbf{E}}^{\mathrm{lin}})^{\mathrm{sym}}$:

$$(\tilde{E}_{IJKL}^{\mathrm{lin}})^{\mathrm{sym}} = \tfrac{1}{2}(\tilde{E}_{IJKL}^{\mathrm{lin}} + \tilde{E}_{KLIJ}^{\mathrm{lin}}) \tag{31}$$

4. LOCALIZATION ANALYSIS

Numerical difficulties have to be faced when softening is included in the material description as in the present model. The boundary-value problem loses ellipticity and the well-known phenomena of localization arise. The numerical solution of the boundary-value problem is mesh dependent and therefore non-unique. Early studies on the localization analysis within the context of acceleration waves have been presented by Hill[15] and only recently by Sluys.[22] The general analysis of localization of plastic deformation in a small band as a presecure to rupture is given by Rice.[23] Some additional fundamental work within the analysis of the post-bifurcation behaviour of soils and concrete can be found in the work of de Borst.[16]

To overcome the mesh dependency, numerous methods and regularization techniques have been proposed such as nonlocal models, rate-dependent models, micropolar models and gradient models. The nonlocal continuum model (Pijaudier-Cabot and Bazant[24]) has been applied to regularize the constitutive equations of the microplane model by Bazant and Ozbolt[14] as well as by Bazant *et al.*[26] A gradient enhanced continuum description for the microplane model has been given only recently by Kuhl *et al.*[26] as well as by De Borst *et al.*[27]

However, regularization methods are not addressed within this study. We will concentrate on the examination of the pointwise onset of localization indicated by the determinant of the acoustic tensor. We begin by summarizing the localization condition. Selected examples will be presented in the following section, to demonstrate the effects of localization in the context of the microplane model.

According to Hill,[15] the assumption of weak discontinuities leads to the existence of a jump in the strain rate field whereas the displacement rates are still continuous:

$$[|\dot{\mathbf{u}}|] = \dot{\mathbf{u}}^+ - \dot{\mathbf{u}}^- = \mathbf{0}, \qquad [|\nabla\dot{\mathbf{u}}|] = \nabla\dot{\mathbf{u}}^+ - \nabla\dot{\mathbf{u}}^- = \xi\mathbf{m}\otimes\mathbf{n} \neq \mathbf{0} \tag{32}$$

Herein $\mathbf{n}$ denotes the normal to the discontinuity surface. The amplitude of the jump is given by ξ and $\mathbf{m}$ is the jump vector defining the mode of localization failure. The traction rate vector, is continuous along the discontinuity surface:

$$[|\dot{\mathbf{t}}|] = \dot{\mathbf{t}}^+ - \dot{\mathbf{t}}^- = \mathbf{0} \tag{33}$$

When inserting the definition of the traction vector $\dot{\mathbf{t}} = [\tilde{\mathbf{E}}^{\mathrm{lin}}:\nabla\dot{\mathbf{u}}]\cdot\mathbf{n}$, equation (33) can be rewritten as follows:

$$\begin{aligned}[|\dot{\mathbf{t}}|] &= \dot{\mathbf{t}}^+ - \dot{\mathbf{t}}^- \\ &= [\tilde{\mathbf{E}}^{\mathrm{lim}+}:\nabla\dot{\mathbf{u}}]\cdot\mathbf{n}^+ - [\tilde{\mathbf{E}}^{\mathrm{lin}-}:\nabla\bar{\mathbf{u}}^-]\cdot\mathbf{n}^- \\ &= [[\tilde{\mathbf{E}}^{\mathrm{lin}+} - \tilde{\mathbf{E}}^{\mathrm{lin}-}]:\nabla\dot{\mathbf{u}}^-]\mathbf{n} - \xi[\mathbf{n}\tilde{\mathbf{E}}^{\mathrm{lin}+}\mathbf{n}]\mathbf{m} = \mathbf{0}\end{aligned} \tag{34}$$

With the assumption of continuous localization, damage increases on both sides of localization zone. The constitutive tensor is thus continuous

$$[|\tilde{\mathbf{E}}^{\mathrm{lin}}|] = \tilde{\mathbf{E}}^{\mathrm{lin}+} - \tilde{\mathbf{E}}^{\mathrm{lin}-} = \mathbf{0} \tag{35}$$

such that the first term of equation (34) vanishes. Therefore, the localization condition reduces to

$$\xi[\mathbf{n}\tilde{\mathbf{E}}^{\mathrm{lin}}\mathbf{n}]\mathbf{m} = \xi\mathbf{q}\mathbf{m} = \mathbf{0} \quad \text{with } \mathbf{q} := \mathbf{n}\tilde{\mathbf{E}}^{\mathrm{lin}}\mathbf{n} \tag{36}$$

Herein $\mathbf{m}$ can be understood as the eigenvector defining the direction of the jump in the strain rate. It characterizes the mode of failure being parallel to $\mathbf{n}$ for mode I failure and perpendicular to $\mathbf{n}$ for mode II failure, respectively. The pointwise onset of localization can be established by analysing the so-called acoustic tensor $\mathbf{q}$, which results in a double contraction of the tangent material operator $\tilde{\mathbf{E}}^{\mathrm{lin}}$ with the normal to the discontinuity surface $\mathbf{n}$. As soon as the determinant of the acoustic tensor becomes negative, localization begins to occur. The direction of the localization zone is given through its normal $\mathbf{n}^{\mathrm{crit}}$, which can be determined by the following minimization problem:

$$\det\mathbf{q}^{\mathrm{crit}} = \min_{\mathbf{n}}[\det\mathbf{q}(\tilde{\mathbf{E}}^{\mathrm{lin}}, \mathbf{n})] = \det[\mathbf{n}^{\mathrm{crit}}\tilde{\mathbf{E}}^{\mathrm{lin}}\mathbf{n}^{\mathrm{crit}}] \leqslant 0 \tag{37}$$

For the two-dimensional case, the vector $\mathbf{n}^{\mathrm{crit}}$ can be expressed in terms of the angle α between the horizontal axis and the normal to the localization zone:

$$\mathbf{n}^{\mathrm{crit}} = [\cos(\alpha^{\mathrm{crit}}), \sin(\alpha^{\mathrm{crit}})]^{\mathrm{T}} \tag{38}$$

In the following examples we will examine the development of the determinant of the acoustic tensor $\mathbf{q}$ and the distribution of damage in different material directions $\mathbf{n}^{\mathrm{crit}}$ for the microplane model.

5. EXAMPLES

5.1. Bar in tension—homogeneous strain distribution

Numerous examples have been studied to identify the microplane parameters describing the material behaviour of concrete. Their results can be found, for example, in papers by Bazant and Prat[9] as well as Ozbolt.[28] We will focus on an example motivated by Bazant and Ozbolt.[14] The response of a concrete specimen is analysed under tension loading resulting in a homogeneous stress state. The specimen which is assumed to develop a plane strain state is loaded by displacement control with incremental load steps of $\Delta u = 0.01$ mm. The numerical integration over the unit circle to obtain the macroscopic stress tensor is performed by 24 integration points. This corresponds to a microplane model with 24 microplanes. The macroscopic parameters E and ν and the additional microplane parameters which are taken from Bazant and Ozbolt[14] can be found in Figure 4.

5.1.1. Temporal development of the localization criterion. Figure 5 shows the load displacement curve of the specimen. The load increases until a critical strain of $\boldsymbol{\varepsilon}^{\text{crit}} = 0.0185\%$ is reached. After the peak load, the load carrying capacity decreases drastically. This behaviour is typical for materials like concrete which show brittle failure after having passed the peak load.

In Figure 6, the determinant of the acoustic tensor is plotted for the different load steps indicated in Figure 5, each for varying orientation angles α. Following the ideas of the localization analysis presented in section 4, the critical angle α^{crit} is the angle corresponding to the minimum value of det $\mathbf{q}$. Obviously, for the homogeneous stress state of this example, localization begins as soon as a softening regime starts. For this particular example, no localization can be found before the peak load is reached, although for a general non-symmetric tangent operator, localization might occur even before the beginning of the softening regime. The critical angle α^{crit} is equal to $0°/180°$. Since this angle characterizes the normal to the localization zone, the localization zone is oriented with an angle of 90° to the loading axis. This corresponds to a pure mode I failure of the

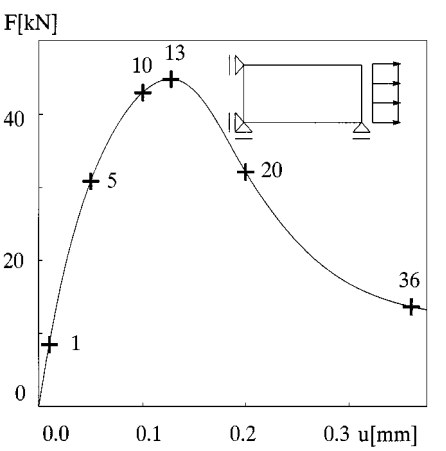

Figure 5. Load displacement curve of concrete bar in tension

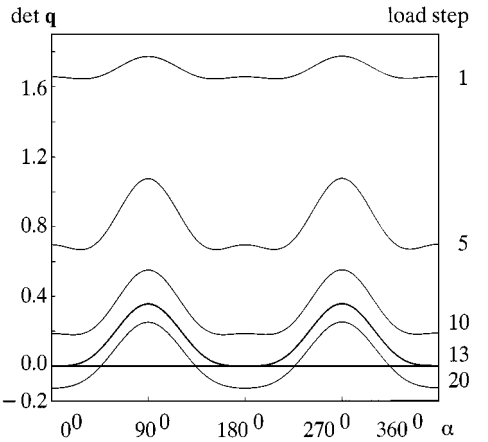

Figure 6. Determinant of acoustic tensor for varying angles α

material as expected. Applying the microplane parameters introduced by Bazant & Ozbolt,[14] the tangential damage variables which characterize shear failure develop much slower than the variables which correspond to normal damage. Since the tangential damage variables have developed slowly at this state, the localization zone spreads perpendicular to the loading axis and the material is subjected to a pure tension failure.

5.1.2. Spatial distribution of the localization criterion compared to microscopic damage evolution. In the second part of the example, we will examine the development of the microplane damage variables in different directions. In order to obtain smoother distributions of the damage variables, 48 microplanes are taken into account (nmp = 48). The specimen geometry and the material parameters are the same as described in the previous example. The following figures show the distribution of volumetric, deviatoric and tangential damage described through the angle α. The presented damage curves of Figures 7–9 and the determinant of the

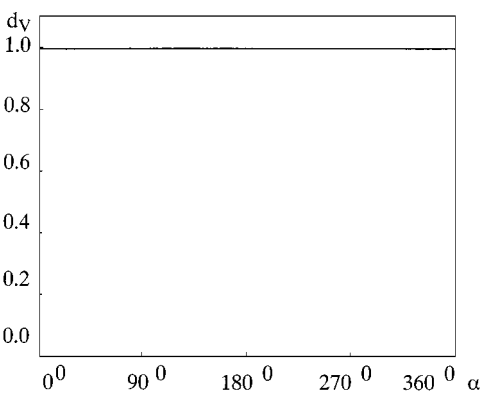

Figure 7. Volumetric damage for varying angles α

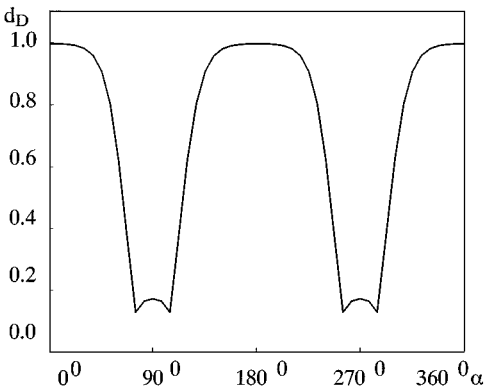

Figure 8. Deviatoric damage for varying angles α

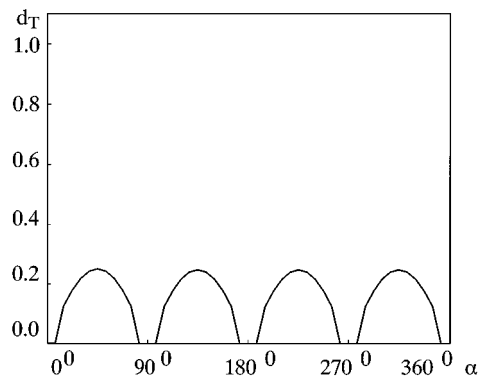

Figure 9. Tangential damage for varying angles α

acoustic tensor of Figure 10 belong to a loading state in the softening regime at $\boldsymbol{\varepsilon} = 0.0514$ (load step 36 in Figure 5).

At $\boldsymbol{\varepsilon} = 0.0514\%$ the volumetric damage, which is displayed in Figure 7, has almost obtained its limit value of one ($d_V = 0.99576$). Since volumetric damage is assumed to be isotropic, it is constant for every direction α. Deviatoric and tangential damage, however, are assumed to develop anisotropically. This can be seen in Figures 8 and 9, where the microscopic variables take different values in different directions indicated through the angle α. Deviatoric damage reaches its maximum values at $\alpha = 0$ and 180° as depicted Figure 8. Under the angle of $\alpha = 0^\circ$ the specimen exhibits pure tension loading. Therefore, this direction has the preference on the normal damage parameters, which almost reach their limit values ($d_D(\alpha = 0^\circ) = 0.99638$). Deviatoric damage results in minimum values at the axis perpendicular to the loading axis.

Figure 9 displays the development of tangential damage which takes maximum values at $\alpha = 45$, 135, 225 and 315°. This result is obvious, because for a specimen under tension loading, these angles represent the directions of pure shear. However, with a maximum value of d_T $(\alpha = 45^\circ) = 0.2511$, tangential damage is far from having reached its limit value of one. This

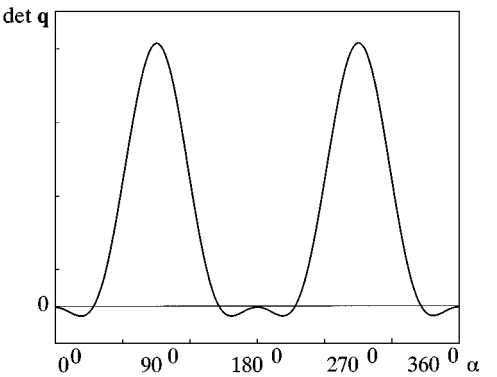

Figure 10. Determinant of $\mathbf{q}$ for varying angles α

corresponds to the results of the first analysis of the example, which showed that the specimen first exhibits tension failure with α^{crit} being equal to 0°. Figure 10 finally reflects the influence of the three different damage variables on the determinant of the acoustic tensor. The critical angle resulting from the distributions of the three damage variables corresponding to $\boldsymbol{\varepsilon} = 0.0514\%$ is at $\alpha^{\text{crit}} = 26^\circ$.

This example clearly shows the physical relevance of the microplane damage parameters. Their maximum values belong to the planes of highest stiffness degradation. With the help of this interpretation, the components of the corresponding fourth-order damage tensor obviously gain a physical relevance.

5.2. Block in tension compression—inhomogeneous stress–strain state

In the second example, the localization criterion will be analysed for a square concrete block. The example simulates a plane strain tension and compression test, whereby the concrete specimen is clamped at its bottom and top. Only one-quarter of the system is analysed. The discretization is performed by 10×10 isoparametric four noded elements since the performance of different element formulations, which is analysed in detail by Steinmann and Willam,[29] is not the scope of this study. Friction at the upper boundary of the system is modelled by not allowing for horizontal displacements, see Figure 11. Inhomogeneity is thus introduced to the boundary-value problem at the upper-left corner, where the strains will concentrate, giving rise to the onset of localization. We will focus on the load–displacement curve of the specimen as well as on the development of the localization criterion for both, tension and compression loading applied by displacement control.

Both load–displacement curves are given in Figures 12 and 13. The most typical characteristic of concrete is quantitatively covered by the model: the critical load in compression is higher than the critical load in tension. Two different failure modes are responsible for the differences of the load deflection curve in tension and the compression curve: concrete in tension fails mainly due to tensile cracking whereas compressed concrete rather fail due to shear. To examine this effect we will analyse the localization criterion for both loading cases. The results are given in Figures 14–17.

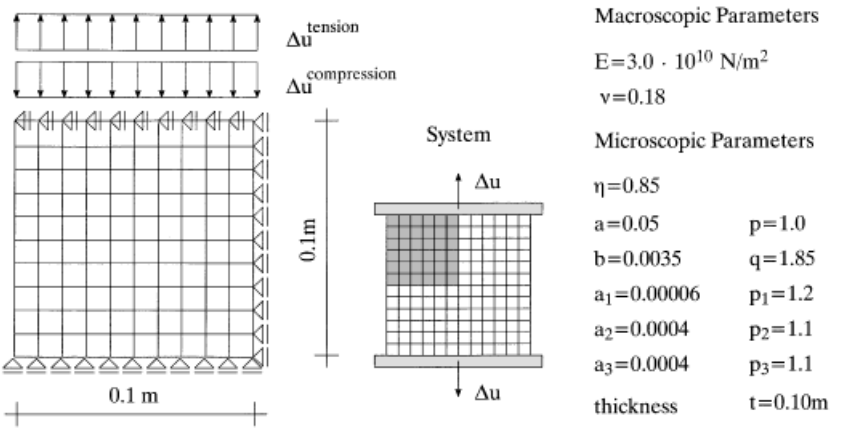

Figure 11. Geometry and parameters of Example 2

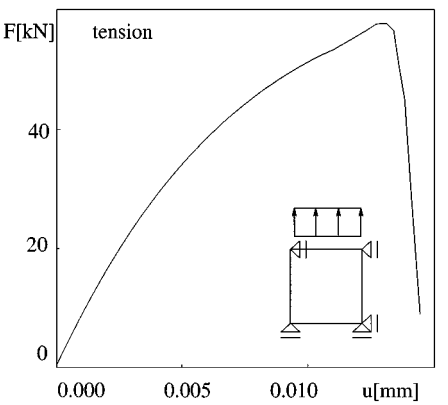

Figure 12. Load–Displacement curve of block in tension

5.2.1. Block in tension. Figure 14 shows the localization zone for the specimen in tension. The different gray scales indicate the sequence of the beginning of localization starting at the dark areas around the integration points in the upper-left corner as enforced by the choice of boundary conditions. Unlike in the homogeneous stress–strain state of Example 5.1, localization begins at a loading situation far before the peak load is reached. The arrows in Figure 14 indicate the direction of the localization zone, calculated by equation (37) as being oriented normal to the vector $\mathbf{n}^{\text{crit}}$. From the calculation, two critical directions can be found, the second being oriented 180° to the first solution $\mathbf{n}^{\text{crit}}$. Since the normal to the localization band is almost perpendicular to the loading axis in every integration point, the structure fails in mode I corresponding to tension failure. This result is confirmed by the calculation of the angle between the critical direction $\mathbf{n}^{\text{crit}}$ and the jump vector $\mathbf{m}$ defining the mode of failure. For this example the two vectors are almost parallel to each other enclosing an angle γ for which $-1^\circ < \gamma\ (\mathbf{n}^{\text{crit}}, \mathbf{m}) < +1^\circ$ in every integration point at the onset of localization.

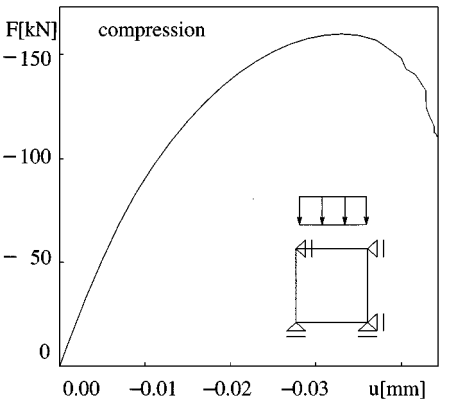

Figure 13. Load–displacement curve of block in compression

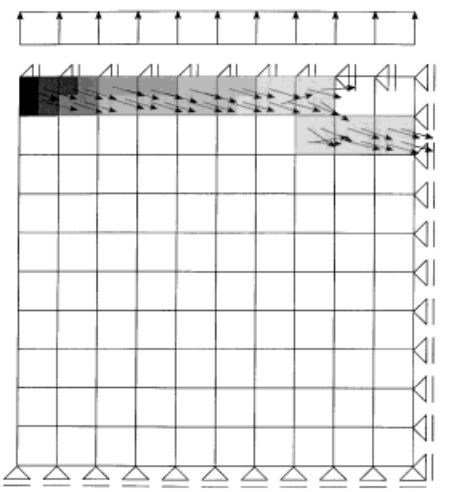

Figure 14. Direction of localization of block in tension

With increased loading, the localization zone spreads horizontally until it has cut the specimen into two parts. This situation corresponds to a sharp drop of the load carrying capacity of the concrete block as indicated in Figure 12. The same numerical phenomenon has been shown by Bazant and Ozbolt[14] for the load–displacement curve of a bar in tension. This corresponds to the loss of ellipticity of the boundary-value problem which then becomes ill-posed. Consequently, an enrichment of the model by regularization techniques will be necessary, since the numerical results for calculations in the post peak regime are not only numerically sensitive but also physically meaningless (de Borst *et al.*[27]).

The distribution of the normal strains in the direction of the loading axis for the loading situation right after the peak load is given in Figure 15. It shows clearly that the strains accumulate in a small band almost perpendicular to the loading axis.

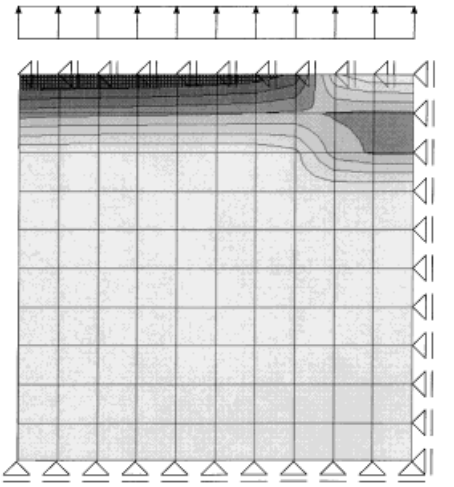

Figure 15. Distribution of strain in loading direction

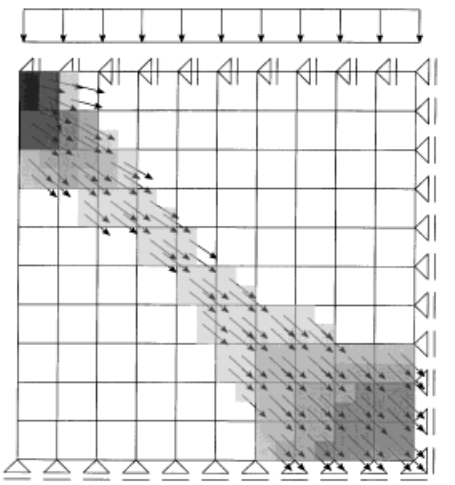

Figure 16. Direction of localization of block in compression

5.2.2. Block in compression. We will now establish the same situation for a block subjected to compression. In Figure 16, the dark areas indicating the beginning of localization are again situated in the upper-left corner. Again, localization begins far before the maximum load is obtained. The arrows in Figure 16 mark one of the four possible critical directions of the localization band calculated by equation (37) in every integration point. For sake of transparency, we only plot one of the possible four directions. The three other critical directions have been calculated being oriented to the marked arrows with an angle of about 90, 180 and 270°, respectively. Unlike in tension where we were able to find only two critical directions, four critical directions can be obtained from the minima of equation (37). In compression loading, the

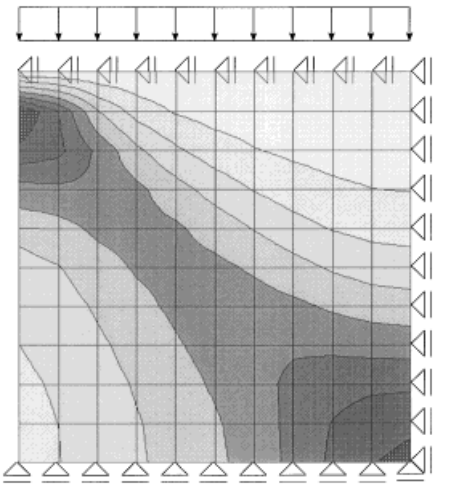

Figure 17. Distribution of strain in loading direction

localization band develops with an angle of about 45° to the loading axis. The pairs of the vectors $\mathbf{n}^{\text{crit}}$ and $\mathbf{m}$ enclose an angle γ being $44^\circ < \gamma < 46^\circ$ at the onset of localization corresponding to a mixed Mode Failure. The orientation of the localization zone is confirmed by the strain distribution of Figure 17. Again, the load carrying capacity is reached, as soon as the localization band has cut the structure into two halves. The analysis of the specimen in compression is dominated by shear failure as expected. This typical phenomenon is predicted by the numerical simulation with the microplane model, which covers a combination of mode I and II failure as shown in this example. However, an interaction of both failure modes on the microplane level has not yet been implemented into this microplane model. A linear dependence of the tangential strains on the volumetric strains has been proposed by Carol *et al.*[12] which was verified experimentally by triaxial tests.

6. CONCLUSION

We have introduced the concept of the microplane model within the framework of continuum damage mechanics. The linearization of the three-dimensional constitutive relation has been presented leading to quadratic convergence of the Newton–Raphson iteration when solving the boundary-value problem. This step is crucial for the efficiency of practical applications of the microplane model in structural analysis. The two-dimensional model has been shown to be incorporated in the constitutive setting in a natural way. The consistent tangent operator has also been applied to a localization analysis indicating the onset of localization through the acoustic tensor. The presented examples demonstrate the features of the microplane model in describing tension as well as shear failure via simple uniaxial stress–strain laws. Furthermore, the localization analysis has been shown capable of explaining the sharp drop in the load deflection curve corresponding to the situation at which the localization band has divided the structure into two parts. It should be mentioned, that regularization techniques are inevitable to be included to keep the boundary-value problem well-posed and to perform a numerical analysis independent of the choice of discretization.

REFERENCES

1. P. H. Feenstra, 'Computational aspects of biaxial stress in plain and reinforced concrete', Ph.D. Thesis, Delft University of Technology, The Netherlands, 1993.
2. L. M. Kachanov, 'Time of rupture process under creep conditions', *Izv. Akad. Nauk SSR, Otd. Tkh. Nauk* **8**, 26–31 (1958).
3. J. L. Chaboche, 'Continuum damage mechanics: part I—general concepts', *J. Appl. Mech.*, **55**, 59–64 (1988).
4. J. L. Chaboche, 'Continuum damage mechanics: part II—damage growth, crack initiation and crack growth', *J. Appl. Mech.*, **55**, 65–72 (1988).
5. J. Lemaitre, 'A course on damage mechanics', *Springer, Berlin* (1992).
6. Z. P. Bazant and P. G. Gambarova, 'Crack shear in concrete: crack band microplane model', *J. Struct. Eng.* ASCE, **110**, 2015–2036 (1984).
7. G. I. Taylor, 'Plastic strain in metals', *J. Inst. Metals*, **62**, 307–324 (1938).
8. M. Ros and A. Eichinger, 'Die Bruchgefahr fester Körper', *Bericht Nr. 172*, Eidgen. Materialprüfungs—und Versuchsanstalt für Industrie, Bauwesen und Gewerbe, EMPA, Zürich, 1949.
9. Z. P. Bazant and P. C. Prat, 'Microplane model for brittle plastic material', I. theory & II. verification. *J. Engng. Mech.*, **114**, 1672–1702 (1988).
10. M. M. Iordache and K. Willam, 'Localized failure modes in cohesive-frictional materials', *Mech. Cohesive-Frictional Mater.* (1997). submitted.
11. S. Weihe, F. Ohmenhäuser and B. Kröplin, 'Anisotropic failure evolution in concrete and other quasi-homogeneous materials due to fracture and slip', *Mech. Cohesive—Frictional Mater.* (1997) submitted.
12. I. Carol, P. Prat and Z. P. Bazant, 'New explicit microplane model for concrete: theoretical aspects and numerical implementation', *Int. J. Solids Struct.*, **29**, 1173–1191 (1992).
13. I. Carol, Z. P. Bazant and P. Prat, 'Geometric damage tensor based on microplane model', *J. Engng Mech.*, **117**, 2429–2448 (1991).
14. Z. P. Bazant and J. Ozbolt, 'Nonlocal microplane model for fracture, damage, and size effects in structures', *J. Engng. Mech.*, **116**, 2485–2505 (1990).
15. R. Hill, 'Acceleration waves in solids', *J. Mech. Phys. Solids*, **10**, 1–16 (1962).
16. R. De Borst, 'Non-linear analysis of frictional materials', Ph.D. Thesis, Delft University of Technology, The Netherlands (1986).
17. I. Carol and P. Prat, 'A multicrack model based on the theory of multisurface plasticity and two fracture energies', *Proc. 4th Int. Conf. Computational Plasticity*, Ed. Owen, Onate, Hinton, Barcelona, 1995, pp. 1583–1594.
18. I. Carol and Z. P. Bazant, 'Damage and plasticity in microplane theory', *Int. J. Solids Struct.*, **34**, 3807–3835 (1997).
19. J. Ozbolt, 'General microplane model for concrete', *Proc. 1st Bolomey Workshop on Numerical Models in Fracture Mechanics of Concrete*, H. Folker, ed., Wittmann, Zürich, 1993, pp. 173–187.
20. Z. P. Bazant and B. H. Oh, 'Microplane model for progressive fracture of concrete and rock', *J. Engng. Mech.*, **111**, 559–582 (1985).
21. A. H. Stroud, *Appropriate Calculation of Multiple Integrals*, Prentice-Hall, Englewood Cliffs, NJ, 1971.
22. L. J. Sluys, 'Wave propagation, localization and dispersion in softening solids', Ph.D. Thesis, Delft University of Technology, The Netherlands, 1992.
23. J. R. Rice, 'The localization of plastic deformation', *Theoretical and Applied Mechanics*, W. T. Koiter ed., North-Holland, Amsterdam, 1976, pp. 207–220.
24. G. Pijaudier-Cabot and Z. P. Bazant, 'Nonlocal damage theory', *J. Engng. Mech.*, **113**, 1512–1533.
25. Z. P. Bazant, J. Ozbolt and R. Eligehausen, 'Fracture size effect: review of evidence for concrete structures', *J. Engng. Mech.*, **120**, 2377–2398 (1994).
26. E. Kuhl, R. De Borst and E. Ramm, 'Anisotropic gradient damage with the microplane model', *Comput. Modelling Concrete Struct.* 231–248 (1988).
27. R. De Borst, M. G. D. Geers, E. Kuhl and R. Peerlings, 'Enhanced damage models for concrete fracture', *Comput. Modelling Concrete Struct.* 103–112 (1998).
28. J. Ozbolt, 'Microplane model for quasibrittle materials—theory and verification', *Report No. 96-1a & 96-1b*, Institut für Werkstoffe im Bauwesen, Universität Stuttgart, 1996.
29. P. Steinmann and K. Willam, 'Performance of enhanced finite element formulations in localized failure computations', *Comput. Methods Appl. Mech. Engng.*, **90**, 845–867 (1991).

